CrossMark
click for updates

Fast fMRI can detect oscillatory neural activity in humans

Laura D. Lewis[a,b,1], Kawin Setsompop[b,c], Bruce R. Rosen[b,c], and Jonathan R. Polimeni[b,c]

[a]Society of Fellows, Harvard University, Cambridge, MA 02138; [b]Athinoula A. Martinos Center for Biomedical Imaging, Massachusetts General Hospital, Boston, MA 02129; and [c]Department of Radiology, Harvard Medical School, Boston, MA 02114

Oscillatory neural dynamics play an important role in the coordination of large-scale brain networks. High-level cognitive processes depend on dynamics evolving over hundreds of milliseconds, so measuring neural activity in this frequency range is important for cognitive neuroscience. However, current noninvasive neuroimaging methods are not able to precisely localize oscillatory neural activity above 0.2 Hz. Electroencephalography and magnetoencephalography have limited spatial resolution, whereas fMRI has limited temporal resolution because it measures vascular responses rather than directly recording neural activity. We hypothesized that the recent development of fast fMRI techniques, combined with the extra sensitivity afforded by ultra-high-field systems, could enable precise localization of neural oscillations. We tested whether fMRI can detect neural oscillations using human visual cortex as a model system. We detected small oscillatory fMRI signals in response to stimuli oscillating at up to 0.75 Hz within single scan sessions, and these responses were an order of magnitude larger than predicted by canonical linear models. Simultaneous EEG–fMRI and simulations based on a biophysical model of the hemodynamic response to neuronal activity suggested that the blood oxygen level-dependent response becomes faster for rapidly varying stimuli, enabling the detection of higher frequencies than expected. Accounting for phase delays across voxels further improved detection, demonstrating that identifying vascular delays will be of increasing importance with higher-frequency activity. These results challenge the assumption that the hemodynamic response is slow, and demonstrate that fMRI has the potential to map neural oscillations directly throughout the brain.

oscillations | hemodynamics | imaging | BOLD

Neuronal information processing is shaped by ongoing oscillatory activity, which modulates excitability in neuronal populations and supports the coordination of large-scale brain networks (1–3). In particular, the occurrence of low-frequency dynamics (0.1–2 Hz) within specific cortical regions has been suggested as a key mechanism underlying perception, attention, and awareness (4, 5), because conscious processes typically evolve on the timescale of hundreds of milliseconds (6) and may depend on cortical dynamics in this frequency range. Localizing >0.1-Hz oscillatory dynamics in the human brain is an essential step toward understanding the mechanisms of the many high-level cognitive processes that occur on these timescales. Studies of the spatial properties of neural oscillations in human subjects have been fundamentally limited by the ill-posed inverse problem of electromagnetic recordings: It is not possible to reconstruct the neural generators of EEG and magnetoencephalography (MEG) signals unambiguously, and signals from deep subcortical structures are rarely detected. Noninvasive neuroimaging approaches that can detect >0.1-Hz oscillations with higher spatial resolution are needed to advance studies of large-scale brain network function.

We hypothesized that recent technical advances in fMRI could potentially enable direct localization of neural oscillations in the human brain. fMRI measures brain function by tracking focal changes in blood flow and oxygenation and therefore is an indirect measure of neuronal activity, with spatial and temporal specificity intrinsically limited by the precision and responsiveness of the coordinated regulation of blood delivery in the brain (7, 8). Typical fMRI experiments use stimuli or tasks designed to elicit large, easily detectable hemodynamic responses, which lag the onset of neuronal activation by several seconds, suggesting that these hemodynamic signals are too slow to capture many aspects of ongoing neuronal activity. However, new MRI technologies available in recent years, such as ultrahigh magnetic field systems, provide boosts in sensitivity, enabling more naturalistic stimulation paradigms that perturb the vasculature only weakly.

In addition to improvements in sensitivity, the recent development of methods for simultaneous multislice (SMS) imaging (9–13) allows whole-brain fMRI to be performed at relatively fast acquisition rates (<1 s). However, the temporal resolution of fMRI has generally been thought to be limited by the sluggishness of the hemodynamic response itself rather than by data-acquisition rates. The slow dynamics of the hemodynamic response function (HRF) result in strong attenuation of high-frequency neural activity (14). In addition, rapidly repeating neural stimuli typically result in smaller fMRI responses (15–20), further limiting the detectability of neural oscillations.

The detection of patterns that are periodic in nature, rather than irregular, is particularly challenging (14). The fMRI response to periodic (nonjittered) stimuli declines rapidly with increasing frequency and has been detected down to a limit of a 6.7-s (21) or 4-s (22) period. Because of the strong attenuation of high-frequency oscillatory signals, event-related fMRI paradigms that use relatively short interstimulus intervals (ISIs) typically either jitter the ISIs or alternate between different stimulus conditions (14, 23). These

Significance

A major challenge in neuroscience is our limited ability to image neural signals noninvasively in humans. Oscillations in brain activity are important for perception, attention, and awareness, and progress in cognitive neuroscience depends on localizing these patterns. fMRI is thought to be too slow to measure brain oscillations because it depends on slow changes in blood flow. Here, we use recently developed imaging techniques to show that fMRI can measure faster neural oscillations than previously thought, and responses are 10 times larger than expected. With computational modeling and simultaneous electroencephalography we show that vascular responses are surprisingly fast when brain activity fluctuates rapidly. These results suggest that fMRI can be used to track oscillating brain activity directly during human cognition.

experimental design choices are made in part to lower the fundamental temporal frequency being studied. In general, the fact that fMRI temporal resolution is limited by slow neurovascular coupling has restricted the majority of fMRI studies to studying dynamics in the <0.1-Hz range, because periodic oscillations above that frequency range are expected to be vanishingly small.

Despite this evidence, recent studies performed during the resting state have suggested that there are significant neuronally driven blood oxygenation level-dependent (BOLD) contributions to fMRI signals at frequencies above 0.1 Hz (24–27). However, a challenge in interpreting fMRI oscillatory dynamics measured during the resting state is that the underlying brain activity is not known. Electrophysiology studies have demonstrated a link between infraslow (<0.1 Hz) EEG activity and the fMRI signal (28, 29), but such studies have not been performed at higher frequencies. In the absence of neurophysiological recordings, it is difficult to ascertain the degree to which the >0.1-Hz fMRI signals are generated by >0.1-Hz neural activity or instead reflect other hemodynamic and physiological processes.

This study aimed to determine whether fMRI signals contain neurally generated oscillatory content above 0.2 Hz and to determine the frequency response to ongoing periodic neural activity. To link the dynamics of the fMRI signal to underlying neural activity, we examined the fMRI response in the context of a known, stimulus-induced neural oscillation and used rapid data acquisition [repetition time (TR) <300 ms] to sample the fMRI oscillatory response directly. We found that fMRI oscillations of up to 0.75 Hz can be detected and that the amplitude of these oscillations is an order of magnitude larger than predicted by canonical models. Using simultaneous EEG–fMRI and model-based simulations, we studied the link between neural activity, neurovascular coupling, and the BOLD signal to determine how fast fMRI responses are generated.

Results

Canonical Linear Models Predict Undetectable fMRI Oscillations at 0.5 Hz.
We used a flickering checkerboard stimulus whose luminance contrast oscillated at a frequency of interest, driving neuronal oscillations in human primary visual cortex (V1) and enabling us to quantify the fMRI response to a controlled oscillation with a known frequency (Fig. 1A).

We first performed simulations of the predicted fMRI response to neural oscillations at each frequency by convolving the idealized neuronal activity (the sinusoidal stimulus waveform) with either the canonical two-gamma HRF used in SPM software, a single-gamma function, or the double-gamma HRF (Fig. 1B) described by Glover (30). The predicted response was estimated as the amplitude of the convolved response once it reached a plateau value (Fig. 1C), discarding the initial transient response. The predicted response amplitude declined exponentially with increasing frequency for all three models (Fig. 1D and Fig. S1A). The amplitude of the fMRI response to a 0.5-Hz neural oscillation was predicted to be 0.8–1.3% of the response to a 0.2-Hz oscillation, suggesting that resolving fMRI signals at delta-range frequencies could be quite challenging. We next added nonlinear effects to the hemodynamic model, because at short ISIs the fMRI response becomes both smaller in amplitude and broader (15, 16, 20), and observed that this nonlinearity is predicted to yield even more temporal smoothing and a further reduction in fMRI signal at higher frequencies (Fig. 1E). However, these models were developed to describe task-evoked activity in response to individual stimuli with long durations during block-design experiments, whereas periodic continuous neural activity, which may be closer to that observed in typical naturalistic contexts, could potentially elicit different hemodynamic responses.

fMRI Oscillations at 0.5 Hz Are an Order of Magnitude Larger than Expected.
To test whether fMRI can detect neural oscillations directly, we acquired fMRI data at 3 T using fast temporal
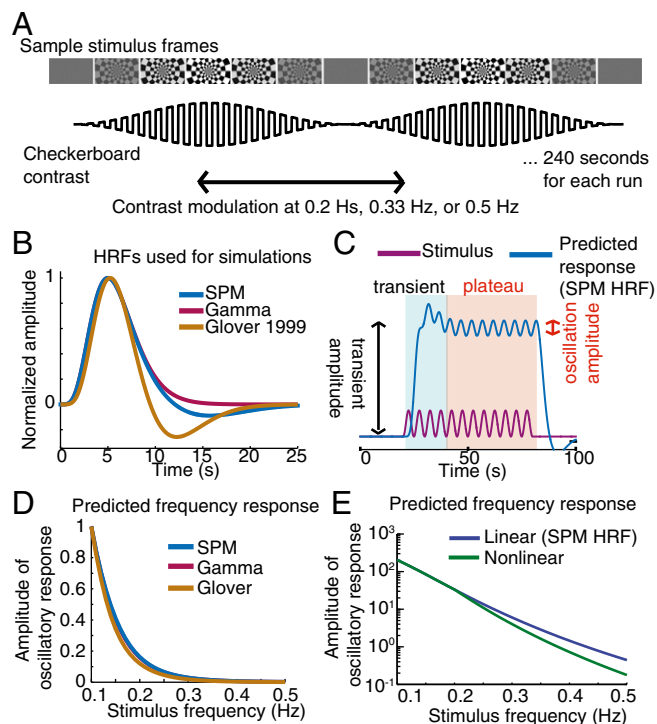

Fig. 1. Linear canonical models predict that the fMRI response to oscillatory neural activity will decrease exponentially as the oscillation frequency increases. (A) Diagram of the visual stimulus. The luminance contrast of a flickering radial checkerboard was modulated at 0.2, 0.33, 0.5, or 0.75 Hz. (B) Time course of the HRFs used for simulations. (C) Example of the predicted fMRI response to sinusoidally oscillating neural activity. As the frequency increases, the predicted response reaches a stable plateau, and the oscillation amplitude around that plateau becomes small. (D) Predicted fMRI response across stimulation frequencies. The predicted response declines exponentially for all HRFs. (E) The predicted fMRI response on a log scale for a linear system and for a sample set of nonlinear parameters shows that nonlinear adaptation effects would be expected to reduce the fMRI response amplitude further at high stimulus frequencies.

sampling (TR ≤280 ms) and analyzed the mean response in V1 during the oscillatory visual stimulus (Fig. 2 A and B). We averaged the mean time series across all voxels in the region of interest (ROI) on every cycle of the stimulus contrast oscillation, discarding the first 3–10 cycles to avoid transient effects (*SI Methods*). The resulting plot shows a stimulus-triggered average of the fMRI data. In experiment 1, we found a robust oscillation in response to the visual stimulation at 0.2 Hz, with an amplitude of 0.73% [95% confidence interval (CI) 0.55, 0.92] (Fig. 2C). As the stimulus frequency increased, we continued to find significant oscillatory responses, with an amplitude of 0.21% (CI 0.09, 0.33) at 0.33 Hz (Fig. 2D) and an amplitude of 0.06% at 0.5 Hz (CI 0.04, 0.09) (Fig. 2E). The induced oscillations also could be seen in the power spectrum of the V1 BOLD signal (Fig. S2), although the evoked analysis (Fig. 2C) enabled a better estimation of oscillation amplitude because it reduced the contribution of non–phase-locked noise. To ensure the replicability of these responses, we conducted a second experiment using SMS imaging to double the number of slices acquired. We again found robust induction of oscillatory responses in V1 when stimulation was delivered at 0.2, 0.33, or 0.5 Hz (Fig. 2 F–H) at similar amplitudes (0.2 Hz = 1.05%, CI 0.83, 1.31; 0.33 Hz = 0.28%, CI 0.15, 0.41; 0.5 Hz = 0.08%, CI 0.04, 0.13). The phase of the response was shifted at higher frequencies, as expected because of the filtering induced by the hemodynamic response (Fig. S1 B and C). Although the response amplitude was small at higher
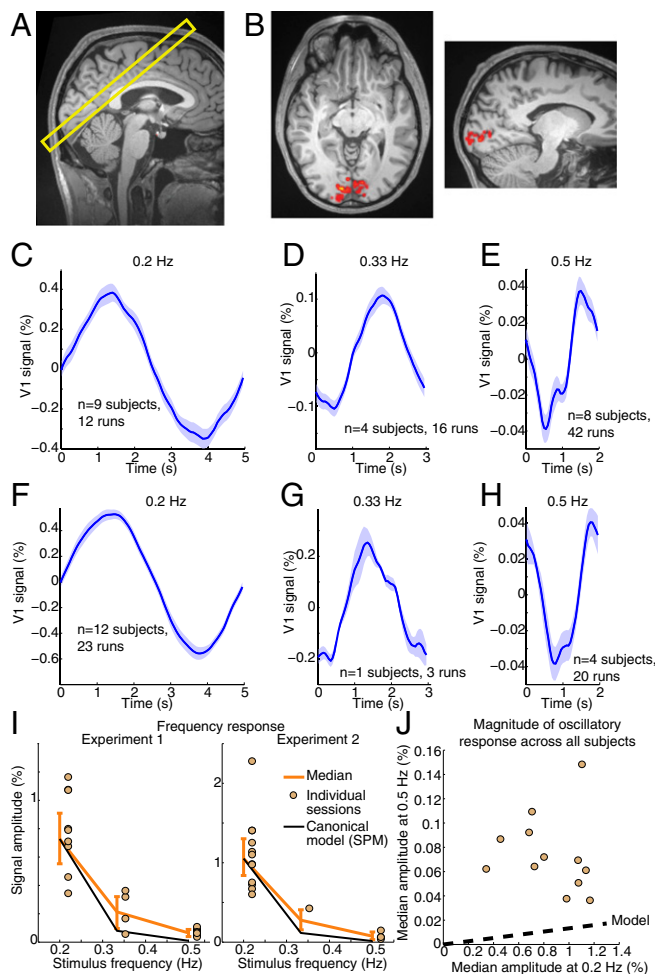
Fig. 2. Oscillatory fMRI responses in V1 acquired at 3 T can be detected at each stimulus frequency and are an order of magnitude larger than predicted. (*A*) An example of slice positioning in experiment 1 (five slices). (*B*) An example of the V1 ROI in a single subject. (*C*) Stimulus-triggered mean response in V1 in experiment 1, locked to the stimulation cycle at 0.2 Hz. The shaded area shows the SE across runs. (*D*) As in *C*, runs at 0.33 Hz. (*E*) As in *C*, runs at 0.5 Hz. (*F–H*) Mean response in V1 in experiment 2. (*I*) Amplitude of the fMRI response across stimulus frequencies, compared with the linear model using the SPM HRF. Error bars are 95% CIs (bootstrap). (*J*) Ratio of the fMRI response at 0.2 Hz to the response at 0.5 Hz across all subjects who participated in both conditions: Each individual subject had a larger response to the 0.5-Hz stimulus than predicted by the canonical linear model with the SPM HRF (black dashed line).

frequencies (Fig. 2*I*), it nevertheless was substantially larger than predicted by the canonical linear model in every subject studied (Fig. 2*J*), eliciting a mean response within individual subjects that was 10.1% the size of the 0.2-Hz condition rather than the 1.3% ratio predicted by the SPM model (*P* = 0.0005, Wilcoxon signed-rank test). The response amplitude was very similar (10.7%) when edge slices were excluded from the analysis, suggesting that these observations were not driven by inflow effects. The fMRI response at 0.5 Hz was therefore an order of magnitude larger than predicted, suggesting that delta-range neuronal oscillations are detected more easily with fMRI than originally thought.

Neural and Vascular Mechanisms Underlying the Unexpectedly Large fMRI Response. The large fMRI response could indicate either that the underlying neural activity is stronger at 0.5 Hz than at 0.2 Hz and so drives a larger hemodynamic response, or that the linear canonical hemodynamic model is not a good fit

for periodic neural activity. To investigate the first possibility, we recorded EEG simultaneously with fMRI in four subjects to obtain an electrophysiological measure of response amplitude. The evoked response was concentrated in occipital channels (Fig. 3*A*), consistent with previous studies suggesting that the steady-state visual evoked potential (SSVEP) is generated largely by visual cortex with strong contributions from V1 (31–33). The cross-correlation between the V1 fMRI signal and the 12-Hz amplitude in the occipital EEG demonstrated a clear correlation (Fig. 3*B*), in line with these previous reports that V1 is a major generator of the SSVEP. The cross-correlation for both stimulus conditions overlapped with a lag of ~3.5 s, suggesting a more rapid hemodynamic response than in canonical models but within a physiologically plausible range.

To determine whether increased neural activity could have contributed to the large fMRI oscillations we observed, we tested how the SSVEP dynamics changed across stimulus frequencies. The stimulus-triggered mean EEG (Fig. 3*C*) contained an evoked signal at 12 Hz (corresponding to the checkerboard contrast inversion frequency), with amplitude modulation of either 0.2 Hz or 0.5 Hz (corresponding to the luminance contrast modulation). The amplitude of the EEG response to the 0.5-Hz stimulus was not larger than the response to the 0.2-Hz stimulus (0.2 Hz = 3.12 μV; 0.5 Hz = 2.99 μV; difference = −0.08; CI −1.4, 1.2) (Fig. 3 *D* and *E*). This finding suggested that the magnitude of the neural response was similar across conditions and that the HRF to ongoing oscillatory neural activity must differ from the classic models developed for transient task activity.

Although the magnitude of neural activity appeared similar across conditions, the duration of neural activity in the 0.5-Hz condition was substantially shorter (Fig. 3 *D* and *E*). fMRI responses are known to exhibit nonlinear dependence on stimulus duration, with briefer stimuli inducing larger responses than expected from a linear system (17, 34, 35). To test the role of stimulus duration explicitly, we presented stimuli with luminance contrast varying as the square of a sinusoidal function, yielding a narrower stimulus waveform than the sinusoidal case (Fig. 4*A*).
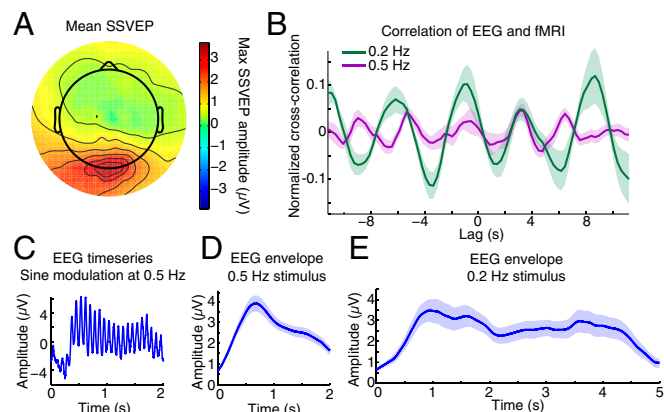

Fig. 3. Simultaneous EEG recordings suggest that the large fMRI responses are not explained by increased amplitude of neural oscillations at higher frequencies. (*A*) The SSVEP to the 0.5-Hz sinusoidal stimulus localizes primarily to occipital channels, consistent with previous studies. (*B*) Cross-correlation of the 12-Hz amplitude in channel OZ and the fMRI signal in the V1 ROI. Both stimulus conditions induce a peak with a lag of ~3.5 s, indicating that the V1 fMRI signal correlates with EEG power at a plausible physiological lag (*n* = 3 subjects, 6 runs at 0.2 Hz, 15 runs at 0.5 Hz). (*C*) Mean EEG across runs with sinusoidal contrast modulation at 0.5 Hz (*n* = 4 subjects, 19 runs) shows an SSVEP at 12 Hz in channel OZ. (*D*) Amplitude envelope of the 12-Hz EEG oscillation across runs at 0.5 Hz (*n* = 4 subjects, 19 runs). (*E*) The amplitude envelope of the 12-Hz EEG across runs at 0.2 Hz has the same magnitude (*n* = 4 subjects, 12 runs).
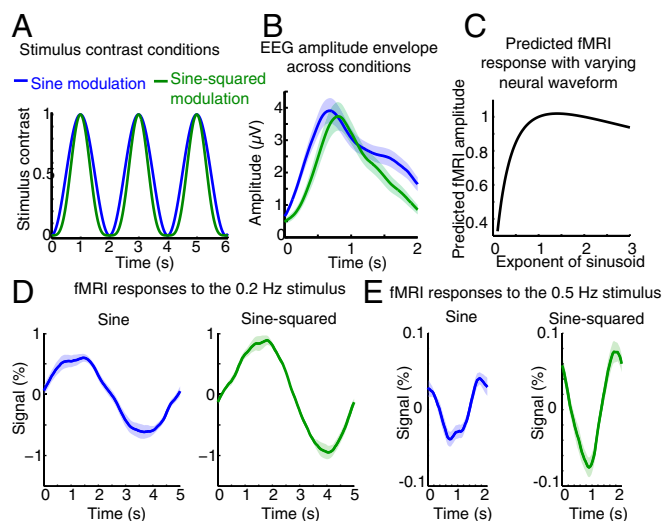
Fig. 4. Continuous and rapidly varying neural activity can elicit faster hemodynamic responses. (*A*) Schematic of the contrast modulation used in the sine vs. sine-squared conditions. In the sine-squared case, the same range of contrasts is used, but the waveform shape is narrower. (*B*) Envelope of the EEG signal. As expected, the magnitude of the EEG is similar across conditions, but the waveform of the EEG response is narrower in the sine-squared case, suggesting successful modulation of the waveform of the underlying neural oscillation. (*C*) The predicted fMRI response to oscillating neural activity varies with its waveform but is expected to change less than 15% in the range of our stimulus parameters. (*D*) The fMRI response to a sine-squared wave at 0.2 Hz is 49% larger than the response to a sine wave. (*E*) Similarly, the fMRI response to a sine-squared wave at 0.5 Hz is 93% larger than the response to a sine wave, demonstrating that narrower neural oscillations drive larger fMRI signals. The shaded region shows the SE across runs.

The EEG recordings in the sine-squared condition had the same magnitude as in the sinusoidal condition (amplitude = 3.12 μV) but had a narrower waveform (Fig. 4*B*), suggesting that this stimulus paradigm successfully elicited neural activity of similar magnitude but briefer temporal dynamics. Simulations predicted that the sine-squared stimulus would elicit a 15% larger fMRI response than the sine stimulus at either stimulus frequency (Fig. 4*C*). In contrast, the measured fMRI response to the sine-squared stimulus was 49% larger (CI 24%, 81%) than the response to the sinusoidal stimulus in the 0.2-Hz stimulus condition (Fig. 4*D*) and was 93% larger (CI 21%, 399%) in the 0.5-Hz stimulus condition (Fig. 4*E*). We concluded that ongoing oscillatory activity can produce relatively large fMRI responses if the waveform of that activity is narrow.

What mechanism could underlie the production of a large fMRI response to >0.1-Hz oscillatory neural activity? A recent study proposed that a faster HRF should be used for resting-state fMRI signals (25). We hypothesized that a fast HRF also should be used for task-driven activity when neural activity varies rapidly and continuously. To test whether a similar modification to the HRF could account for our data, we simulated the predicted fMRI response using HRFs with different shapes. Narrower HRFs produced larger responses at high stimulus frequencies: An HRF peaking at 2.5 s predicted a response at 0.5 Hz that is five times larger than the canonical SPM HRF (Fig. S3 *A* and *B*). In addition, the 93% increase in fMRI signal observed for the sine-squared vs. sine modulation at 0.5 Hz could be generated if the HRF shape depends on the duration of the neural activity, because an additional reduction of the HRF width would generate this increase (Fig. S3*B*). A single parsimonious model in which the temporal dispersion of the HRF is linked to the timescale of neural activity could therefore explain these data.

Biophysical Modeling of Oscillatory fMRI Responses. To test whether this narrower shape for the HRF is physiologically plausible during task-evoked neural activity, we implemented the balloon model (36–38) and examined its responses to a brief input. We considered two possible factors that could contribute to a faster HRF in this experiment: (*i*) whether brief neural activity induces a narrower fMRI response, as suggested by Fig. 4, and (*ii*) whether continuous, rather than transient, activity would affect the shape of the response. To test the first possibility, we examined the predicted responses to a single cycle of a sinusoidal flow input with increasing frequency (Fig. S3*C*). We varied the time constant for the viscoelastic effect, in which blood volume transiently lags before achieving steady state. Setting this time constant to zero, as in the original model, yielded slow BOLD responses similar to the canonical HRF (Fig. 5*A* and Fig. S3*D*). However, when this time constant was set to physiologically plausible nonzero values (37), the BOLD response to stimuli of shorter duration was both faster (time-to-peak) and narrower (FWHM) (Fig. 5*A* and Fig. S3*E*). These sharper dynamics demonstrate that when cerebral blood volume (CBV) lags changes in cerebral blood flow (CBF) rather than maintaining a steady-state relationship, the fMRI response to high frequencies or brief activity is expected to increase.

Another possibility is that continuous periodic stimuli may shift the system to a new steady state in which baseline flow is higher and the system can respond more rapidly to changes in neural activity. Higher baseline flow would reduce the mean transit time, used as a time constant in the balloon model. Varying this parameter demonstrated that higher baseline flow would speed up the BOLD response (Fig. S3*F*), although the effects were less than those seen when the viscoelastic parameter was varied. However, values near 2 s, which would be consistent with prior reports (39), were sufficient to replicate the responses we observed, suggesting that as long as the mean transit time is relatively short at baseline, these oscillations could be expected.

When using the modified balloon model with these parameter settings to simulate the response to the visual stimulus, we obtained predictions much closer to the data: The model predicted that the fMRI response amplitude to a 0.5-Hz stimulus should be 7.5% of the response to a 0.2-Hz stimulus (Fig. 5 *B* and *C*), compared with ~8–10% in the data (whereas the canonical model predicted 1.3%). These analyses demonstrated that a physiologically grounded model can produce the responses we observed, through viscoelastic effects that cause blood volume to lag while changes in flow vary more rapidly, leading to a sharpened HRF waveform when neural activity is brief. The large fMRI responses we observed therefore may be explained by a shift in the shape of the
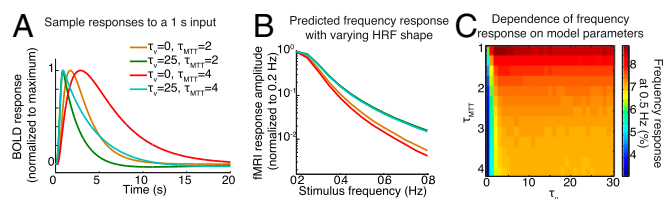

Fig. 5. Modeling suggests that the vasculature can respond relatively quickly to oscillatory neural activity. (*A*) Predicted responses to a 1-s sine flow input using different parameters for the balloon model. (*B*) The predicted frequency response demonstrates that modifying the time constants within physiological values is expected to lead to an order-of-magnitude increase in fMRI oscillatory responses. (*C*) The predicted amplitude at 0.5 Hz (normalized to 0.2 Hz), depending on balloon model parameters. Low but still plausible values for the mean transit time (τ_{MTT}) and the increased viscoelastic constant (τ_v) lead to values closer to the data (~8%, orange/red region of the plot).

HRF, with continuous and rapidly varying neural activity inducing a sharper HRF and thereby leading to rapid fMRI responses.

Extending Detection of Oscillatory Activity up to 0.75 Hz. This model also allowed us to extrapolate and generate predictions of the fMRI response at even higher frequencies, predicting that stimuli at 0.75 Hz would elicit a response 1.9% as large as the response at 0.2 Hz (as opposed to 0.14% predicted by the linear convolutional model). Our experiments at 3 T were unable to detect a significant neural response to the 0.75-Hz oscillation (amplitude, 0.02%; CI –0.02, 0.06), because the noise was larger than the predicted signal. To increase the signal-to-noise ratio, we conducted a third experiment at 7 T. We found a significant fMRI oscillation during 0.75-Hz stimulation (Fig. 6 *A* and *B*) with an amplitude of 0.021% (CI 0.009, 0.034). This value corresponded to 1.46% of the signal at 0.2 Hz, i.e., slightly below the balloon model prediction but an order of magnitude larger than the canonical model. The phase of the response again was shifted within a range that would be expected with physiologically plausible models (Fig. S4). To control for the possibility that the detected oscillation was caused by a physiological or motion artifact rather than by neural activation, we analyzed a control gray matter region that was not visually driven and observed no significant oscillation (amplitude, 0.002%; CI –0.006, 0.010) (Fig. 6 *C* and *D*). In addition, the 0.75-Hz oscillation in V1 was still detectable when physiological noise was reduced through nuisance regression of white matter and ventricle signals (Fig. S5). The magnitude of the observed response was small but nevertheless was detectable within a single session of scanning at 7 T, suggesting that the fMRI response is measurable and larger than predicted even at 0.75 Hz.

Accounting for Vascular Delays Improves Resolution of Neural Oscillations. The analyses described up to this point were averaged across all visually responsive voxels in V1, assuming similar response properties throughout that region. However, HRFs vary across the brain (40), and the structure of local vasculature can alter the timing of responses in individual voxels by hundreds of milliseconds (41). As stimulation frequencies approach 0.5 Hz (i.e., a period of 2 s), these delays can introduce cancellation into fMRI signals when averaging is performed across voxels. We therefore examined the response phase in individual voxels. In the localizer run, we selected voxels with the earliest peak response (in the 0–33rd percentile) and voxels with the latest peak response (in the 67th–100th percentile, median lag 635 ms). We then analyzed the response of these voxels on the other functional runs (Fig. 7*A*). In the 3-T experiments, the late-responding

voxels exhibited a signal 97% larger than the early-responding voxels in the 0.2-Hz condition ($P = 0.0004$) and 54% larger in the 0.5-Hz condition ($P = 0.02$). Late and large-amplitude responses typically correspond to larger draining veins (41), suggesting that even large veins can contain periodic oscillatory signals at frequencies 0.2 Hz.

The phase delays across voxels suggest that identifying and correcting for hemodynamic delays could further improve the detection of oscillatory signals. In the 0.75-Hz condition, separating early- and late-responding voxels had a large impact, because these lags introduced major phase cancellation when averaged across all voxels (Fig. 7*B*). The mean signal amplitude in the early-responding voxels alone was 0.033%, 45% larger than the results from averaging across all voxels within the ROI (Fig. 7*C*). Furthermore, this result was better aligned with the model prediction from the data generated at lower frequencies (0.027%). Overall, late-responding voxels exhibited a more severe drop-off in signal as stimulus frequency increased, and early-responding voxels exhibited slightly larger responses at 0.75 Hz (Fig. 7*D*), suggesting that high-frequency oscillatory activity may be detected more easily in voxels with rapid response onset. The oscillations in early-responding voxels were also significant ($P < 0.05$) within a single scan session in three of the five subjects, in addition to the mean being significant across the group. The early- and late-responding voxels were spatially intermixed (Fig. 7*E*), suggesting that avoiding spatial smoothing during preprocessing and then grouping individual voxels according to their lags in a localizer run before analysis can further improve the detectability of high-frequency oscillations.

Discussion

We conclude that the fMRI response to oscillatory neural activity is detectable up to at least 0.75 Hz within a single 7-T scan session in individual subjects, and higher frequencies may be detectable with future gains in MRI sensitivity. The amplitude of the fMRI signal at high frequencies is an order of magnitude larger than predicted by canonical linear models, suggesting that fMRI could provide a new method for noninvasively localizing oscillatory neural activity in the human brain. The strong oscillatory responses result from the faster dynamics of the BOLD response when neural activity is continuous and rapidly varying, suggesting that different models of the hemodynamic response should be used in studies seeking to analyze ongoing periodic activity or rapidly fluctuating activity rather than large, transient task-evoked activations. The HRFs derived from these conventional block-design stimulation paradigms do not represent a true "impulse response" in the strict sense of the term; instead, for rapid stimulus presentations, the shape of the HRF varies as a function of the stimulus duration. The slow canonical hemodynamic response functions may reflect the slow experimental paradigms used to obtain them, whereas hemodynamic responses to rapidly fluctuating neural activity are, in fact, fast. This interpretation also could explain the observations of previous studies that have reported nonlinear fMRI responses to short-duration stimuli (17, 25, 34, 42). We suggest that, rather than representing a problem for fMRI because of the failure of the canonical linear models, these fast responses in fact mean that fMRI has an unexpectedly strong ability to measure naturalistic, rapidly varying neural activity. Updated models with faster HRFs may provide a generally better representation of the true hemodynamic response during high-level cognitive tasks, because it is likely that cortical activity typically is ongoing at fluctuating rates rather than slowly alternating between the silent and high firing rates that can be induced in primary sensory cortices through a blocked experimental design.

Our model suggests that both viscoelastic effects and a new vascular baseline state during rapid neural activity could contribute to the fast dynamics we observed. The fact that increasing the variability in neural firing rates through a narrower stimulus waveform (Fig. 4) increased the fMRI response amplitude suggests
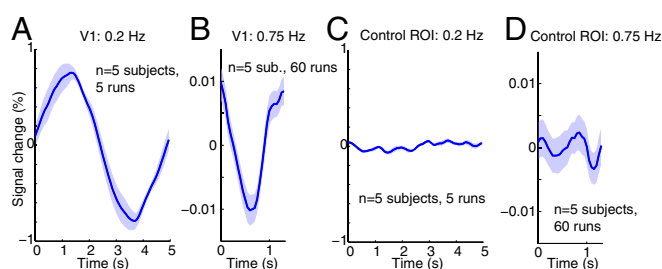

Fig. 6. fMRI responses can be detected reliably up to 0.75 Hz. (*A*) In experiment 3, at 7 T, oscillatory stimuli at 0.2 Hz evoked consistent and large responses. (*B*) At 0.75 Hz, the evoked oscillations were still statistically detectable and were ~1% of the amplitude of the 0.2-Hz signal. (*C* and *D*) A non-visually activated gray matter control ROI does not show oscillatory responses, suggesting that the detected oscillation is caused by neural activity rather than by motion or physiological noise. In all panels, the shaded region shows the SE across runs.
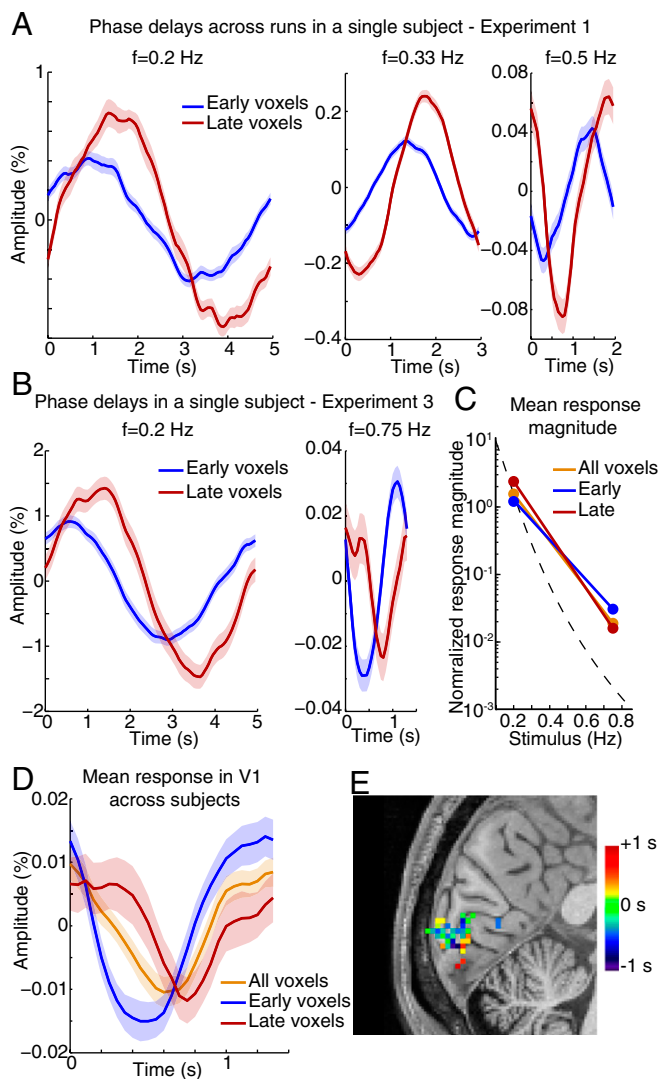
Fig. 7. Accounting for vascular lags can further improve the resolution of fMRI oscillations. (*A*) Responses of early-responding and late-responding voxels across stimulus frequencies in an individual subject. The phase delays persist across conditions, and the fMRI response is larger in the later-responding voxels. (*B*) Early- and late-responding voxels plotted for a subject in experiment 3. At 0.75 Hz, the lags across voxels introduce phase cancellation of the fMRI response. The shaded region shows the SE across cycles. (*C*) The mean oscillatory response across all subjects in experiment 3 declines more in late-responding voxels and is stronger in early-responding voxels at high frequencies. The black dashed line is the prediction of the canonical linear model. (*D*) Mean time series across subjects in experiment 3 demonstrates that analyzing the early voxels separately results in larger oscillations than are detectable when averaging across the whole V1 ROI (*n* = 5 subjects, 60 runs). The shaded region is standard error across runs. (*E*) Heterogeneous spatial distribution of lags in individual voxels. The image is from a representative subject. Color indicates the phase lag in each voxel in the localizer run.

that the HRF waveform depends on the dynamic activity patterns of the neurons. The important influence of viscoelastic effects suggests that classic block designs induce steady-state dynamics with a slow HRF, whereas uncoupling of CBF and CBV during dynamic neural activity leads to a sharper HRF and stronger frequency response. Although we could not directly measure the CBF responses to these fast oscillations because of the limited temporal resolution and sensitivity of arterial spin-labeling methods, previous experiments have demonstrated that the CBF–CBV coupling is altered during dynamic stimulation (43) and have suggested that

the CBV lags during dynamic neural activity; this suggestion is consistent with our proposed model. Further studies will be needed to assess the mechanism underlying our results more conclusively. Experiments manipulating total flow using hypercapnia or caffeine have found that the shape of the hemodynamic response changes in a counterintuitive manner that does not match model predictions (44, 45); however, these agents also influence neuronal activity and oxygen consumption (46, 47) and may act through different pathways than neuronal activity (48). Directly manipulating CBF and/or neural activity would be valuable for testing the underlying mechanism. Although selectively manipulating a single parameter of the vasculature is not feasible in humans, studies in animal models could manipulate either local neuronal activity or local vessel dilation while performing simultaneous flow and neuronal imaging to test these mechanisms causally.

We also show that the impact of hemodynamic delays is severe when studying signals above 0.1 Hz, because the delays typically seen in vasculature can be hundreds of milliseconds (41, 42, 49), large enough to cause phase cancellation in rapidly oscillating signals. Spatial smoothing can therefore attenuate oscillatory fMRI signals substantially, because the delay in neighboring voxels can differ according to their local vascular anatomy. Analysis methods that take local vascular delays into account (15, 50–52) will be essential when analyzing fast fMRI activity. Smaller voxel sizes also could improve the resolution of higher frequencies, although fMRI's spatial resolution is also limited by its point spread function. Ultimately, high-spatial-resolution scans are expected to yield better results when studying fast neural activity, because they would minimize smoothing across regions with different phase delays. Current fMRI analyses are weighted toward the large (and hence slow) signals from draining veins, and shifting to focus selectively on the rapidly responding voxels, which exhibited less attenuation at high frequencies, may enhance the detection of faster neural dynamics.

Our results suggest that fMRI now can be used to measure oscillatory neural activity on the timescale of many high-level cognitive processes, in the hundreds of milliseconds. Even higher frequencies potentially could be attained when averaging across sufficient numbers of subjects and sessions, and animal studies directly imaging the vasculature could test the upper limit of hemodynamic oscillatory responses. The temporal resolution of fMRI undoubtedly will still be limited, because it seems unlikely the vasculature follows rapid neural oscillations (e.g., >10 Hz), but our results suggest it could be useful for measuring dynamics in the slow-delta range. In particular, this approach could be used to measure endogenous low-frequency oscillations and <1-Hz modulations of gamma power, dynamics that are key to modulating attention and states of consciousness (4, 53–55). Intracranial recordings in human subjects (54, 56) have demonstrated that slow oscillatory activity is often spatially isolated, but these invasive methods can access only restricted cortical regions and are limited to patient populations. Similarly, amplitude modulation of high-frequency oscillations occurs locally and on timescales of hundreds of milliseconds, putting it in the range of phenomena that can be measured and spatially localized using this approach. Fast fMRI studies potentially could resolve the spatial distribution of these dynamics across the entire cortex and in subcortical structures simultaneously, yielding new insight into the role of oscillatory neural dynamics in human cognition.

Methods

Written informed consent was obtained from all subjects, and all experimental procedures were approved by the Massachusetts General Hospital Institutional Review Board. Experiment 1 included data from seven subjects, and experiment 2 included data from nine subjects, using a Siemens Tim Trio 3T scanner and similar stimulus paradigms but different imaging acquisition parameters. Experiment 3 included five subjects and was conducted on a Siemens Magnetom whole-body 7-T scanner. For four subjects in experiment

2 we also acquired a simultaneous EEG using an Electrical Geodesics 256-channel system. Visual stimuli consisted of a 12-Hz (inversion rate) flickering checkerboard with luminance contrast modulation oscillating at the frequency of interest. Displayed fMRI time series show the mean fMRI data triggered on each cycle of the visual stimulus. Statistics for the magnitude of the fMRI oscillation were computed using a nonparametric bootstrap to estimate the 95% CIs. Full details of acquisition and analysis procedures are provided in *SI Methods*.

1. Buzsáki G, Draguhn A (2004) Neuronal oscillations in cortical networks. *Science* 304(5679):1926–1929.
2. Fries P (2005) A mechanism for cognitive dynamics: Neuronal communication through neuronal coherence. *Trends Cogn Sci* 9(10):474–480.
3. Uhlhaas PJ, Singer W (2010) Abnormal neural oscillations and synchrony in schizophrenia. *Nat Rev Neurosci* 11(2):100–113.
4. He BJ, Raichle ME (2009) The fMRI signal, slow cortical potential and consciousness. *Trends Cogn Sci* 13(7):302–309.
5. Lakatos P, Karmos G, Mehta AD, Ulbert I, Schroeder CE (2008) Entrainment of neuronal oscillations as a mechanism of attentional selection. *Science* 320(5872):110–113.
6. Dehaene S, Changeux J-P (2011) Experimental and theoretical approaches to conscious processing. *Neuron* 70(2):200–227.
7. O'Herron P, et al. (2016) Neural correlates of single-vessel haemodynamic responses in vivo. *Nature* 534(7607):378–382.
8. Logothetis NK (2008) What we can do and what we cannot do with fMRI. *Nature* 453(7197):869–878.
9. Larkman DJ, et al. (2001) Use of multicoil arrays for separation of signal from multiple slices simultaneously excited. *J Magn Reson Imaging* 13(2):313–317.
10. Feinberg DA, et al. (2010) Multiplexed echo planar imaging for sub-second whole brain fMRI and fast diffusion imaging. *PLoS One* 5(12):e15710.
11. Moeller S, et al. (2010) Multiband multislice GE-EPI at 7 tesla, with 16-fold acceleration using partial parallel imaging with application to high spatial and temporal whole-brain fMRI. *Magn Reson Med* 63(5):1144–1153.
12. Setsompop K, et al. (2012) Blipped-controlled aliasing in parallel imaging for simultaneous multislice echo planar imaging with reduced g-factor penalty. *Magn Reson Med* 67(5):1210–1224.
13. Barth M, Breuer F, Koopmans PJ, Norris DG, Poser BA (2016) Simultaneous multislice (SMS) imaging techniques. *Magn Reson Med* 75(1):63–81.
14. Dale AM (1999) Optimal experimental design for event-related fMRI. *Hum Brain Mapp* 8(2-3):109–114.
15. Friston KJ, Josephs O, Rees G, Turner R (1998) Nonlinear event-related responses in fMRI. *Magn Reson Med* 39(1):41–52.
16. Huettel SA, McCarthy G (2000) Evidence for a refractory period in the hemodynamic response to visual stimuli as measured by MRI. *Neuroimage* 11(5 Pt 1):547–553.
17. Pfeuffer J, McCullough JC, Van de Moortele P-F, Ugurbil K, Hu X (2003) Spatial dependence of the nonlinear BOLD response at short stimulus duration. *Neuroimage* 18(4):990–1000.
18. Birn RM, Bandettini PA (2005) The effect of stimulus duty cycle and "off" duration on BOLD response linearity. *Neuroimage* 27(1):70–82.
19. de Zwart JA, et al. (2009) Hemodynamic nonlinearities affect BOLD fMRI response timing and amplitude. *Neuroimage* 47(4):1649–1658.
20. Liu Z, et al. (2010) Linear and nonlinear relationships between visual stimuli, EEG and BOLD fMRI signals. *Neuroimage* 50(3):1054–1066.
21. Thomas CG, Menon RS (1998) Amplitude response and stimulus presentation frequency response of human primary visual cortex using BOLD EPI at 4 T. *Magn Reson Med* 40(2):203–209.
22. Bandettini PA, Cox RW (2000) Event-related fMRI contrast when using constant interstimulus interval: Theory and experiment. *Magn Reson Med* 43(4):540–548.
23. Dale AM, Buckner RL (1997) Selective averaging of rapidly presented individual trials using fMRI. *Hum Brain Mapp* 5(5):329–340.
24. Lin F-H, et al. (2015) Significant feed-forward connectivity revealed by high frequency components of BOLD fMRI signals. *Neuroimage* 121(C):69–77.
25. Chen JE, Glover GH (2015) BOLD fractional contribution to resting-state functional connectivity above 0.1 Hz. *Neuroimage* 107(C):207–218.
26. Boubela RN, et al. (2013) Beyond noise: Using temporal ICA to extract meaningful information from high-frequency fMRI signal fluctuations during rest. *Front Hum Neurosci* 7:168.
27. Lee H-L, Zahneisen B, Hugger T, LeVan P, Hennig J (2013) Tracking dynamic resting-state networks at higher frequencies using MR-encephalography. *Neuroimage* 65(C):216–222.
28. He BJ, Snyder AZ, Zempel JM, Smyth MD, Raichle ME (2008) Electrophysiological correlates of the brain's intrinsic large-scale functional architecture. *Proc Natl Acad Sci USA* 105(41):16039–16044.
29. Picchioni D, et al. (2011) Infraslow EEG oscillations organize large-scale cortical-subcortical interactions during sleep: A combined EEG/fMRI study. *Brain Res* 1374:63–72.
30. Glover GH (1999) Deconvolution of impulse response in event-related BOLD fMRI. *Neuroimage* 9(4):416–429.
31. Vialatte F-B, Maurice M, Dauwels J, Cichocki A (2010) Steady-state visually evoked potentials: Focus on essential paradigms and future perspectives. *Prog Neurobiol* 90(4):418–438.
32. Bianciardi M, et al. (2009) Single-epoch analysis of interleaved evoked potentials and fMRI responses during steady-state visual stimulation. *Clin Neurophysiol* 120(4):738–747.
33. Di Russo F, et al. (2007) Spatiotemporal analysis of the cortical sources of the steady-state visual evoked potential. *Hum Brain Mapp* 28(4):323–334.
34. Yeşilyurt B, Uğurbil K, Uludağ K (2008) Dynamics and nonlinearities of the BOLD response at very short stimulus durations. *Magn Reson Imaging* 26(7):853–862.
35. Birn RM, Saad ZS, Bandettini PA (2001) Spatial heterogeneity of the nonlinear dynamics in the fMRI BOLD response. *Neuroimage* 14(4):817–826.
36. Buxton RB, Wong EC, Frank LR (1998) Dynamics of blood flow and oxygenation changes during brain activation: The balloon model. *Magn Reson Med* 39(6):855–864.
37. Buxton RB, Uludağ K, Dubowitz DJ, Liu TT (2004) Modeling the hemodynamic response to brain activation. *Neuroimage* 23(Suppl 1):S220–S233.
38. Mildner T, Norris DG, Schwarzbauer C, Wiggins CJ (2001) A qualitative test of the balloon model for BOLD-based MR signal changes at 3T. *Magn Reson Med* 46(5):891–899.
39. Obata T, et al. (2004) Discrepancies between BOLD and flow dynamics in primary and supplementary motor areas: Application of the balloon model to the interpretation of BOLD transients. *Neuroimage* 21(1):144–153.
40. Handwerker DA, Ollinger JM, D'Esposito M (2004) Variation of BOLD hemodynamic responses across subjects and brain regions and their effects on statistical analyses. *Neuroimage* 21(4):1639–1651.
41. Yu X, et al. (2012) Direct imaging of macrovascular and microvascular contributions to BOLD fMRI in layers IV-V of the rat whisker-barrel cortex. *Neuroimage* 59(2):1451–1460.
42. de Zwart JA, et al. (2005) Temporal dynamics of the BOLD fMRI impulse response. *Neuroimage* 24(3):667–677.
43. Simon AB, Buxton RB (2015) Understanding the dynamic relationship between cerebral blood flow and the BOLD signal: Implications for quantitative functional MRI. *Neuroimage* 116(C):158–167.
44. Cohen ER, Ugurbil K, Kim S-G (2002) Effect of basal conditions on the magnitude and dynamics of the blood oxygenation level-dependent fMRI response. *J Cereb Blood Flow Metab* 22(9):1042–1053.
45. Liu TT, et al. (2004) Caffeine alters the temporal dynamics of the visual BOLD response. *Neuroimage* 23(4):1402–1413.
46. Zappe AC, Uludağ K, Oeltermann A, Uğurbil K, Logothetis NK (2008) The influence of moderate hypercapnia on neural activity in the anesthetized nonhuman primate. *Cereb Cortex* 18(11):2666–2673.
47. Xu F, et al. (2011) The influence of carbon dioxide on brain activity and metabolism in conscious humans. *J Cereb Blood Flow Metab* 31(1):58–67.
48. Iadecola C (2004) Neurovascular regulation in the normal brain and in Alzheimer's disease. *Nat Rev Neurosci* 5(5):347–360.
49. Saad ZS, Ropella KM, Cox RW, DeYoe EA (2001) Analysis and use of FMRI response delays. *Hum Brain Mapp* 13(2):74–93.
50. Liao CH, et al. (2002) Estimating the delay of the fMRI response. *Neuroimage* 16(3 Pt 1):593–606.
51. Calhoun VD, Stevens MC, Pearlson GD, Kiehl KA (2004) fMRI analysis with the general linear model: Removal of latency-induced amplitude bias by incorporation of hemodynamic derivative terms. *Neuroimage* 22(1):252–257.
52. Chang C, Thomason ME, Glover GH (2008) Mapping and correction of vascular hemodynamic latency in the BOLD signal. *Neuroimage* 43(1):90–102.
53. Massimini M, Tononi G, Huber R (2009) Slow waves, synaptic plasticity and information processing: Insights from transcranial magnetic stimulation and high-density EEG experiments. *Eur J Neurosci* 29(9):1761–1770.
54. Lewis LD, et al. (2012) Rapid fragmentation of neuronal networks at the onset of propofol-induced unconsciousness. *Proc Natl Acad Sci USA* 109(49):E3377–E3386.
55. Schroeder CE, Lakatos P (2009) Low-frequency neuronal oscillations as instruments of sensory selection. *Trends Neurosci* 32(1):9–18.
56. Nir Y, et al. (2011) Regional slow waves and spindles in human sleep. *Neuron* 70(1):153–169.
57. Brainard DH (1997) The psychophysics toolbox. *Spat Vis* 10(4):433–436.
58. Kleiner M, Brainard D, Pelli D (2007) What's new in Psychtoolbox-3? *Perception* 36(14):1–16.
59. van der Kouwe AJW, Benner T, Salat DH, Fischl B (2008) Brain morphometry with multiecho MPRAGE. *Neuroimage* 40(2):559–569.
60. Polimeni JR, et al. (2016) Reducing sensitivity losses due to respiration and motion in accelerated echo planar imaging by reordering the autocalibration data acquisition. *Magn Reson Med* 75(2):665–679.
61. Greve DN, Fischl B (2009) Accurate and robust brain image alignment using boundary-based registration. *Neuroimage* 48(1):63–72.
62. Fischl B (2012) FreeSurfer. *Neuroimage* 62(2):774–781.
63. Fischl B, et al. (2008) Cortical folding patterns and predicting cytoarchitecture. *Cereb Cortex* 18(8):1973–1980.
64. Hinds O, et al. (2009) Locating the functional and anatomical boundaries of human primary visual cortex. *Neuroimage* 46(4):915–922.
65. Bokil H, Andrews P, Kulkarni JE, Mehta S, Mitra PP (2010) Chronux: A platform for analyzing neural signals. *J Neurosci Methods* 192(1):146–151.
66. Niazy RK, Beckmann CF, Iannetti GD, Brady JM, Smith SM (2005) Removal of FMRI environment artifacts from EEG data using optimal basis sets. *Neuroimage* 28(3):720–737.
67. Delorme A, Makeig S (2004) EEGLAB: An open source toolbox for analysis of single-trial EEG dynamics including independent component analysis. *J Neurosci Methods* 134(1):9–21.
68. Havlicek M, et al. (2015) Physiologically informed dynamic causal modeling of fMRI data. *Neuroimage* 122(C):355–372.
69. Friston KJ, Mechelli A, Turner R, Price CJ (2000) Nonlinear responses in fMRI: The Balloon model, Volterra kernels, and other hemodynamics. *Neuroimage* 12(4):466–477.